Cascade CO_2 electroreduction enables efficient carbonate-free production of ethylene

Ozden, Adnan; Wang, Yuhang; Li, Fengwang; Luo, Mingchuan; Sisler, Jared; Thevenon, Arnaud; Rosas-Hernández, Alonso; Burdyny, Thomas; Lum, Yanwei; More Authors

DOI
10.1016/j.joule.2021.01.007

Publication date
2021

Document Version
Accepted author manuscript

Published in
Joule

Citation (APA)
Ozden, A., Wang, Y., Li, F., Luo, M., Sisler, J., Thevenon, A., Rosas-Hernández, A., Burdyny, T., Lum, Y., & More Authors (2021). Cascade CO_2 electroreduction enables efficient carbonate-free production of ethylene. *Joule*, *5*(3), 706-719. https://doi.org/10.1016/j.joule.2021.01.007

Cascade CO_2 electroreduction enables efficient carbonate-free production of ethylene

Adnan Ozden[1†], Yuhang Wang[2†], Fengwang Li[2†], Mingchuan Luo[2], Jared Sisler[2], Arnaud Thevenon[3], Alonso Rosas-Hernández[3], Thomas Burdyny[4], Yanwei Lum[2], Hossein Yadegari[1], Theodor Agapie[3], Jonas C. Peters[3], Edward H. Sargent[2] & David Sinton[1]**

[1]*Department of Mechanical and Industrial Engineering, University of Toronto, 5 King's College Road, Toronto, Ontario, M5S 3G8, Canada.*

[2]*Department of Electrical and Computer Engineering, University of Toronto, 10 King's College Road, Toronto, Ontario, M5S 3G4, Canada.*

[3]*Joint Center for Artificial Photosynthesis and Division of Chemistry and Chemical Engineering, California Institute of Technology, Pasadena, California, 91125, USA.*

[4]*Department of Chemical Engineering, Delft University of Technology, Van der Maasweg 9 2629 HZ Delft, The Netherlands.*

†These authors contributed equally to this work.

**Correspondence and requests for materials should be addressed to David Sinton (D.S.) (sinton@mie.utoronto.ca) and Edward H. Sargent (E.H.S.) (ted.sargent@utoronto.ca).*

SUMMARY

CO_2 electroreduction (CO_2RR) to multi-carbon products such as ethylene (C_2H_4) provides a route to produce valuable products and reduce CO_2 emissions. Despite improvements in catalytic performance, the direct transformation of CO_2-to-C_2H_4 suffers from CO_2 loss to carbonate. This CO_2 reactant loss is a major driver of cost, consuming up to 72% of total energy input. A cascade approach – coupling a solid-oxide CO_2-to-CO electrochemical cell (SOEC) with a CO-to-C_2H_4 membrane electrode assembly (MEA) electrolyser – would eliminate CO_2 loss to carbonate. However, this approach requires CO-to-C_2H_4 in an MEA electrolyser with energy efficiency well beyond demonstrations to date. Focusing on the MEA, we find that the organic film produced from the reduction of N-tolylpyridinium to N-tolyl-tetradihydro-bipyridine improves the stabilization of key reaction intermediates, while an SSC ionomer enhances CO transport to the Cu surface, allowing for the stable production of C_2H_4 at higher selectivities. We achieve a C_2H_4 Faradaic efficiency (FE) of 65% at a current density of 166 mA cm^{-2} over 110 hours of operation. Demonstrating a full cascade SOEC-MEA approach, we achieve CO_2-to-C_2H_4 with no loss of CO_2 to carbonate and a total energy requirement of ~138 GJ (tonne C_2H_4)$^{-1}$, which represents a ~48% reduction in energy intensity compared to the direct route. We further couple CORR with glucose electrooxidation that enables carbonate formation-free C_2H_4 production with a full-process energy requirement of ~89 GJ (tonne C_2H_4)$^{-1}$.

Keywords

CO electroreduction, carbon utilization, ethylene electrolysis, electrolyser, membrane electrode assembly, solid oxide electrolyser, catalyst design, molecular catalyst, energy efficiency.

INTRODUCTION

Global annual ethylene (C_2H_4) production reached 185 Mt in 2018, exceeding that of any other organic chemical.[1] Production of C_2H_4 involves steam cracking of fossil fuel-derived long-chain hydrocarbons – a process that releases 2-3 tonnes of CO_2 per tonne of C_2H_4 produced before the in-plant CO_2 capture.[2] The net process releases ~200 Mt of CO_2 annually,[1] accounting for 0.6% of total anthropogenic emissions.[3]

CO_2 electroreduction (CO_2RR) using renewable electricity holds promise for low-carbon C_2H_4 production.[4] Present day CO_2RR has reached Faradaic efficiencies (FEs) of 70-80% towards C_2H_4[5-7] and energy efficiencies (EEs) over 30% at current densities over 100 mA cm^{-2}.[5] However, due to the formation of carbonate during CO_2RR (Figure S1), concerns regarding the consequent penalty in energy consumption and production cost have risen.[8,9]

To assess the energy and cost associated with CO_2 reactant loss to carbonate, we performed energy and techno-economic assessments (TEA) for benchmark neutral and alkaline CO_2RR systems from literature, with the ideal and base case scenarios (Notes S1, S2, Figures S2, S3, S4, S5 and Tables S1 and S2). Electrolyte regeneration, system operation, and anodic product separation associated with carbonate formation significantly increases energy consumption and cost. The regeneration of alkaline electrolyte induces a penalty of ~278 GJ per tonne C_2H_4 produced, accounting for 60-70% of the total energy requirement (Figures 1A, B). Membrane electrode assembly (MEA) electrolysers result in less carbonate formation. However, six moles CO_3^- for every mole of C_2H_4 is produced, leading to a 4× increase in membrane resistance,[10] pH-gradient induced high voltages,[11] and 60-90 GJ of additional energy consumption per tonne C_2H_4 – a process energy penalty of ~35% (Figures 1A, B and Tables S1, S2).

Encouraged by recent advances in CO electroreduction,[8,9] we took the view that carbonate-

free conversion of CO_2 to C_2H_4 could be realized through two cascading steps (Figure 1C): (I) CO_2 reduction to CO in a high-temperature CO_2-to-CO electrochemical cell (SOEC) which avoids carbonate formation[12] and (II) CO reduction to C_2H_4 (CORR-to-C_2H_4) in an MEA electrolyser (Figure S6). Despite the cascade approach requiring additional energy input for separation and heating, as well as two separate systems, the cascade route could be competitive with the direct route (employing best-reported metrics in literature as inputs and assuming capital costs fixed to $/kW, Table S1). The cascade approach benefits from high process efficiency in the SOEC step, as well as the use of an alkaline electrolyte in the CO-to-C_2H_4 step, without suffering carbonate formation (Table S1 – Cell Voltage). For both electroproduction routes, operating potential, FE and current density are the most important parameters influencing the energy intensity of C_2H_4 production (Figure S7).

RESULTS AND DISCUSSION

CO_2-to-CO conversion in an SOEC

We established first the performance of CO_2-to-CO in an SOEC. The SOEC was operated at 800ºC. 95% CO FE and 89% CO EE were achieved at 815 mA cm^{-2} and a CO_2 flow rate of 20 sccm (Figure 2A). This is equal to a CO_2-to-CO single-pass efficiency of ~36%. Utilization can be further improved by lowering flow rates or increasing current, to the limit imposed by the CO disproportionation reaction, also referred to as the Boudouard reaction.[13,14] Here, a maximum CO_2-to-CO single-pass efficiency of ~55% was obtained (Figure 2B) at a CO FE of ~77%, current density of 1.25 A cm^{-2}. At lower flow rates, considering both CO selectivity and CO_2 single-pass conversion, the current density vs. CO_2 flow rate ratio of 815:15 (mA cm^{-2}:sccm) was confirmed to be the best condition under which we observed a constant CO FE of ~91% and CO_2-to-CO single-pass conversion of ~45% (Figure 2C). The energy input requirement for this SOEC step was 13.49 GJ/tonne CO.

CORR MEA for C_2H_4 electroproduction

For C_2H_4 production, our analysis shows that the success of this two-step approach relies on CO-to-C_2H_4 in an MEA electrolyser (Figures S3-S5). High C_2H_4 FE (> 60%) is required in concert with high current density (>150 mA cm^{-2}) and low operating full-cell potential (< 3 V). To date, the highest FE for CO-to-C_2H_4 in MEA electrolysers remains below 40%, and the corresponding C_2H_4 partial current density (j_{C2H4}) is less than 60 mA cm^{-2}.[8] We therefore sought to develop a high performance CO-to-C_2H_4 MEA electrolyser that is essential for efficient, cascade CO_2-to-C_2H_4 conversion.

We first electrodeposited copper (Cu) catalysts under CO_2-rich conditions as MEA cathodes. A CO_2-rich environment increases Cu(100) exposure,[15] which enhances the selectivity towards C_2H_4 in CO_2RR.[8,16] However, a simple Cu surface has large regions that do not have ready access to CO on the hydrophilic surface (Figure S8A).[17] We assembled the MEA – using electrodeposited Cu as the cathode electrode, anion exchange membrane as the solid state electrolyte, and iridium oxide supported on a titanium mesh as the anode electrode – and investigated the CORR performance. This catalyst consequently favors H_2 production, allowing C_2H_4 production with a maximum FE of only 50% at a low partial current density (j_{C2H4}) of 60 mA cm^{-2} (Figure S8B).

Modifying the Cu surface with hydrophobic aliphatic molecules or ionomers has been demonstrated to increase reactant availability at the catalytic interface[17-19] and improve the selectivity and activity towards C_2H_4 electroproduction[20]. We therefore added a $(C_4HF_7O_4S\ .C_2F_4)_x$ short-side-chain (SSC) ionomer coating on the Cu surface.[21] We found that H_2 selectivity was suppressed by 10-30% across the screened cell potential window, and that the highest j_{C2H4} increased to ~155 mA cm^{-2} (Figure S9). However, the maximum C_2H_4 FE remained ~50%.

The strategy we pursued to promote C_2H_4 at lower potentials was to alter the adsorption of the key CO* intermediate via a molecular tuning strategy.[6] We therefore introduced an *N-tolyl substituted tetrahydro-bipyridine* (labeled Py) interlayer between Cu and SSC by an electro-dimerization method.[6] This metal:molecular film:ionomer combination (labeled Cu:Py:SSC), in which SSC improves the CO diffusion at the outer layer and Py provides more atop-bound CO* on Cu surface (Figure 3A), enabled the highest C_2H_4 FE of 65 ± 1% at a 2.5 V full-cell potential and provided a j_{C2H4} of 130 mA cm^{-2} at 2.6 V (Figure 3B). Detailed CORR-to-C_2H_4 performance of the Cu:Py:SSC, Cu:SSC, and bare Cu are summarized in Tables S3-S5. To gain insight into the enhanced CO-to-C_2H_4 selectivity and productivity, we investigated the catalysts using scanning and transmission electron microscopy (SEM and TEM, respectively). We observed a dendritic Cu fully covered by the Py molecule and SSC ionomer (Figure 3C and Figure S10). The Cu catalyst has high crystallinity, confirmed by the grazing-incidence wide-angle X-ray scattering (GIWAXS) (Figure S11). We conclude that there was full coverage of Py and SSC on the Cu surface.

We then conducted *operando* Raman spectroscopic studies on the catalytic interface.[22-25] We observed a stabilized atop-bound CO*,[6] known to favor the key CO-CO dimerization step,[26-28] evidenced by the transformation of CO* adsorption configurations (Figure S12): the fraction of the area of atop-bound CO* at the wave number of ~2080 cm^{-1} [29] increased to 33% when Py molecule was electrodeposited onto the Cu surface. By contrast, bridge-bound CO* at 1980-2020 cm^{-1} [29-31] dominated the adsorption configurations on the bare Cu.

We then sought to optimize the full-cell EE by increasing the alkalinity of the anolyte (Figure 3D and Tables S6-S8). With increasing KOH concentration, the C_2H_4 FE peak increased to ~65% (Figure 3D), an example of alkalinity favoring C_{2+} production.[5,32,33] The ionic conductivity was also improved by high alkalinity, and the j_{C2H4} at each C_2H_4 FE peak

increased from ~47 to ~100 mA cm^{-2}, and the full-cell potential reduced from 2.8 to 2.5 V in the range of 0.1 to 3 M KOH (Figure 3D, Figure S13, and Tables S5-S7). However, 5 M KOH lowered the j_{C2H4} to 81 mA cm^{-2} at all applied potentials (Figure S14 and Table S8), which we attribute to a low CO concentration at the catalyst layer under this condition (Figure S15). Considering C_2H_4 FE, j_{C2H4}, and full-cell potential, the 3 M KOH is the best anolyte for CO-to-C_2H_4 conversion in this system.

Further comparisons in 3 M KOH revealed that the Cu:Py:SSC combination outperformed the Cu:SSC and bare Cu in terms of both j_{C2H4} and C_2H_4 full-cell EE (Figure 3E). Importantly, we achieve – when compared to bare Cu – a 5x increase in the peak j_{C2H4} (from 26±2 to 129±1 mA cm^{-2}) and a 1.4x increase in the peak full-cell EE (from 21±2 to 29±1%) using the Cu:Py:SSC combination (Tables S3 and S5). We observed typical CORR gas and liquid products in the current density range of 25 to 250 mA cm^{-2}, with the peak C_{2+} FE of ~85% at 160 mA cm^{-2} (Table S9 and Figure S16). A stable 28% C_2H_4 full-cell EE for the Cu:Py:SSC system was achieved in the current density range of 80 to 170 mA cm^{-2}, whereas the Cu:SSC and bare Cu systems were limited to EEs of <20% in this current density range (Figure 3E). Further optimization of the CO coverage on the Cu:Py:SSC catalyst – through co-feeding CO with N_2 – improved the C_2H_4 full cell EE to 30±1% at a constant current density of 100 mA cm^{-2} (Table S10).

We investigated the C_2H_4 production rate (R_{C2H4}) and its concentration in the product stream. The Cu:Py:SSC combination produced C_2H_4 at almost 0.68 mmol cm^{-2} h^{-1} and 1.5 and 6 times faster than the Cu:SSC and bare Cu, respectively (Figure S17). Using an inlet CO flow rate of 4 sccm, we obtained a ~36% C_2H_4 concentration in gas products (Figure 3F and Table S11). This translated to a ~26% CO-to-C_2H_4 single-pass conversion and is ~3 times higher than that of bare Cu.

We confirmed the stability of the MEA with the Cu:Py:SSC catalyst using 3 M KOH at 150 mA cm^{-2}. The system maintained a constant C_2H_4 FE of 61 ± 2% and a full-cell potential of 2.73 ± 0.02 V for 110 hours with no performance degradation (Figure 3G). We analyzed the cathode electrode after 110-hour continuous electrolysis, using electron microscopy, X-ray photon spectroscopy, and soft X-ray adsorption spectra (sXAS) at the N K-edge. The Cu morphology and Py:SSC coating as well as associated features were retained (Figures S18, S19, and S20). The MEA equipped with the Cu:Py:SSC catalyst – when taking the carbonate formation penalty into account – outperformed literature benchmarks[6,8,11,34-36] including both CO_2RR and CORR, in C_2H_4 FE, j_{C2H4}, C_2H_4 full-cell EE and operation duration (Table S12).

Cascade CO_2-to-C_2H_4 electroreduction in the integrated system

We built an integrated system for carbonate-free CO_2-to-C_2H_4 electroproduction (Figure 1C) by combining the high-performance CO-to-C_2H_4 MEA with the CO_2-to-CO SOEC. The SOEC was operated at 800°C and a current density of 550 mA cm^{-2}, yielding a ~95% CO FE, ~86% CO full-cell EE (for electricity only), and ~48% single-pass utilization (Figure S21). The inlet CO_2 flow rate was set at 10 sccm to ensure the optimal 815:15 (mA cm^{-2} vs. sccm) ratio of current density: CO_2 flow rate and an outlet CO production of ~4.5 sccm for a high CO-to-C_2H_4 single-pass conversion utilization. The products of the SOEC were purified using CO_2 capture solution containing 30% ethanolamine before feeding into the CO-to-C_2H_4 MEA. The temperature of the purified gas supplied to the MEA electrolyser was measured to be 25 °C. The system had a peak CO_2-to-C_2H_4 EE (for electricity only) of 20% (Figure 4A) and a maximum single-pass conversion of ~11% for CO_2-to-C_2H_4 with no loss of CO_2 to carbonate formation in electrolytes (Figure 4B). The combined system produced C_2H_4 at a peak rate of 1.3 mmol h^{-1} at 120 mA cm^{-2} (Figure 4C), along with a C_{2+} FE of ~76% (Table S13). The system maintained the peak single-pass conversion and productivity in CO_2-to-C_2H_4 at 120 mA

cm^{-2} for 40 hours of uninterrupted operation (Figure 4D). The full cascade system achieved carbonate-free electroproduction of C_2H_4 with an energy intensity of 138 GJ (tonne C_2H_4)$^{-1}$, a major savings relative to the direct route (~267 GJ (tonne C_2H_4)$^{-1}$) (Table S20).

Having established the system performance in side-by-side comparison with previous on-step CO_2R processes, we take the MEA in the cascade system a step further. We replaced the oxygen evolution reaction (OER) with the glucose electrooxidation reaction (GOR) for which the thermodynamic potential is ~1 V less than that of OER.[37] We detected gluconate, glucuronate, glucarate, and formate – all products with values higher than that of glucose – as the major GOR products in the current density range of 40 to 200 mA cm^{-2} (Table S14 and Figure S22). We found that coupling the CORR and GOR in alkaline media reduces the potential requirement approximately 1 V at industrially relevant current densities (Figures 4E and S23 and Tables S15-18). At a current density of 120 mA cm^{-2}, we obtained a C_2H_4 FE of ~55% and a C_{2+} FE of ~90% at an MEA full-cell potential of 1.27 V (Figure 4E and Tables S17 and S19). This voltage reduction enables a total energy requirement of ~89 GJ (tonne C_2H_4)$^{-1}$, which represents a 35% reduction in the energy consumption compared to the MEA cell using OER anode at the same current density (~138 GJ (tonne C_2H_4)$^{-1}$) (Table S20). All earlier comparisons involve OER only, both in the cascade system and all reference cases. This additional GOR result highlights the potential to reduce the energy intensity of C_2H_4 production further. Herein, we also note that although the anodic products – gluconate, glucuronate, glucarate, and formate – are more valuable than the glucose input, making a full economic case for the anode side upgrading would require detailed assessment of multiple separations, which is beyond the scope of this work.

Despite the gains demonstrated here, profitable C_2H_4 electroreduction with cascade CO_2RR will require further improvements in performance metrics, including selectivity, current density,

single pass utilization, energy efficiency – in both the first step (CO_2-to-CO in SOEC) and second step (CO-to-C_2H_4 in MEA) (Note S3 and Table S20). Further reductions in the capital and operational costs of both systems will also bring the C_2H_4 electroproduction closer to viability (Note S3 and Table S20).

CONCLUSIONS

We developed a cascade approach to CO_2-to-C_2H_4 conversion that avoids carbonate formation and associated energy penalties, combining an SOEC with a high performance CORR MEA system designed here. We designed a layered catalyst structure composed of a metallic Cu, N-tolyl-tetrahydro-bipyridine, and SSC ionomer to achieve high-rate and efficient CO-to-C_2H_4 conversion in a MEA electrolyser. The combined functions of each layer raised the device C_2H_4 FE to 65%, at a full-cell C_2H_4 EE of 28% across a broad range of current densities, versus the <50% FEs of the bare and single-layer catalyst structures. To drive an end-to-end CO_2 conversion process without the loss of CO_2 to carbonate, we paired our MEA electrolyser with a SOEC for CO_2-to-CO conversion. With the CO stream produced from the SOEC, the MEA system generated C_2H_4 at a peak rate of 1.3 mmol h^{-1} and maintained continuous operation for 40 hours. The full cascade system required ~138 GJ (tonne C_2H_4)$^{-1}$, achieving significant savings over the directly-comparable one-step CO_2-to-C_2H_4 route (~267 GJ (tonne C_2H_4)$^{-1}$). Having established the direct comparison with existing systems on the basis of OER anode reactions in all cases, we devised an approach to reduce the energy consumption of the MEA further, switching the OER anode to GOR. With this enhancement, the cascade SOEC-MEA system requires a total energy requirement of ~89 GJ (tonne C_2H_4)$^{-1}$. These results demonstrate the potential to electrocatalytically convert CO_2 to C_2H_4 without carbonate production and associated energy penalties. The result is a record-low energy requirement for the production of the world's most-produced organic compound.

FIGURES

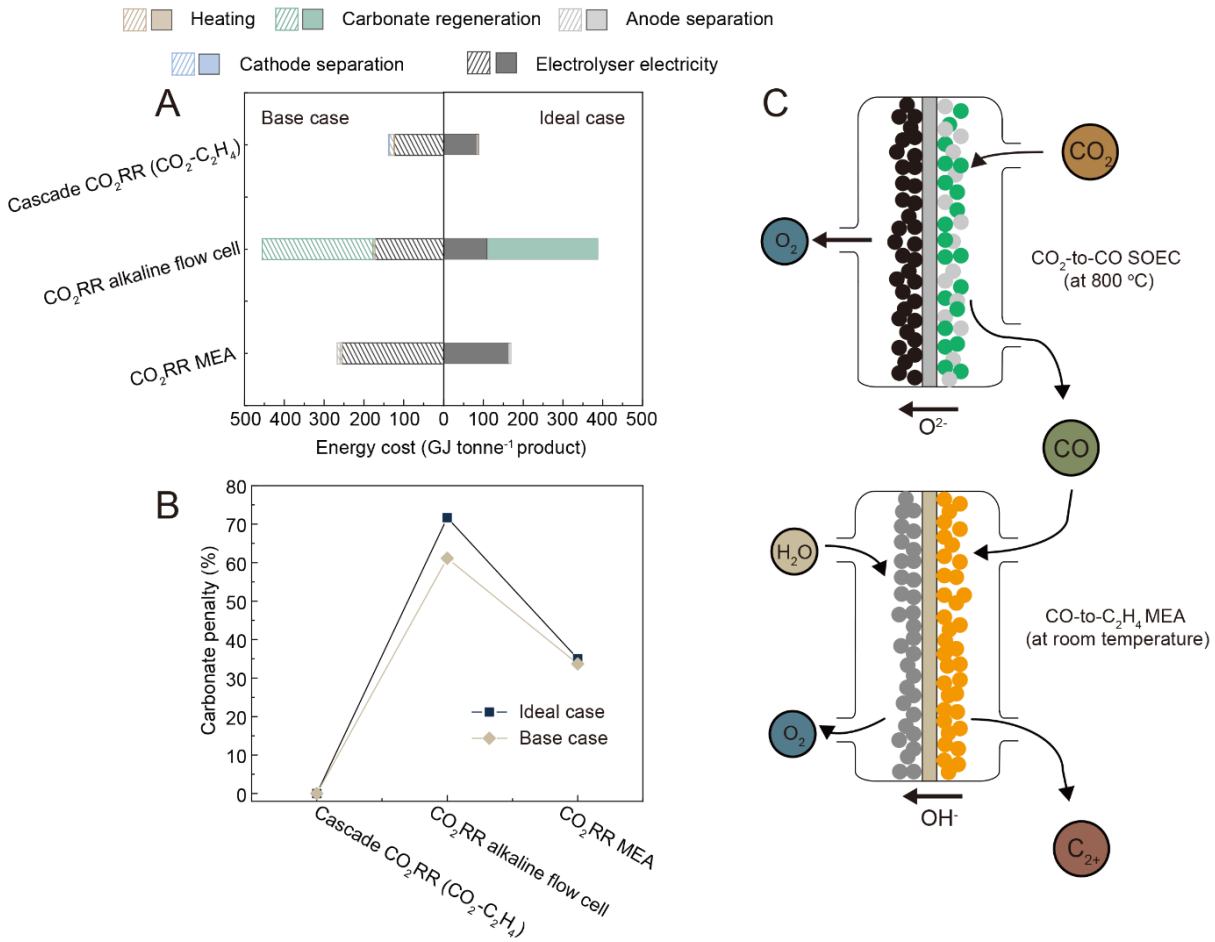

Figure 1. Carbonate-formation-free CO_2-to-C_2H_4 production through cascade CO_2RR.

(A) Comparison of energy comsumption for C_2H_4 production in various systems. **(B)** The carbonate penalty (i.e., the faction of energy comsumption due to carbonate formation) in the various systems. TEA calculation details are provided in the supplementary information. **(C)** A schematic illustration of renewable CO_2-synthesized C_2H_4 in a combined system consisting of a CO_2-to-CO SOEC and a CO-to-C_2H_4 MEA.

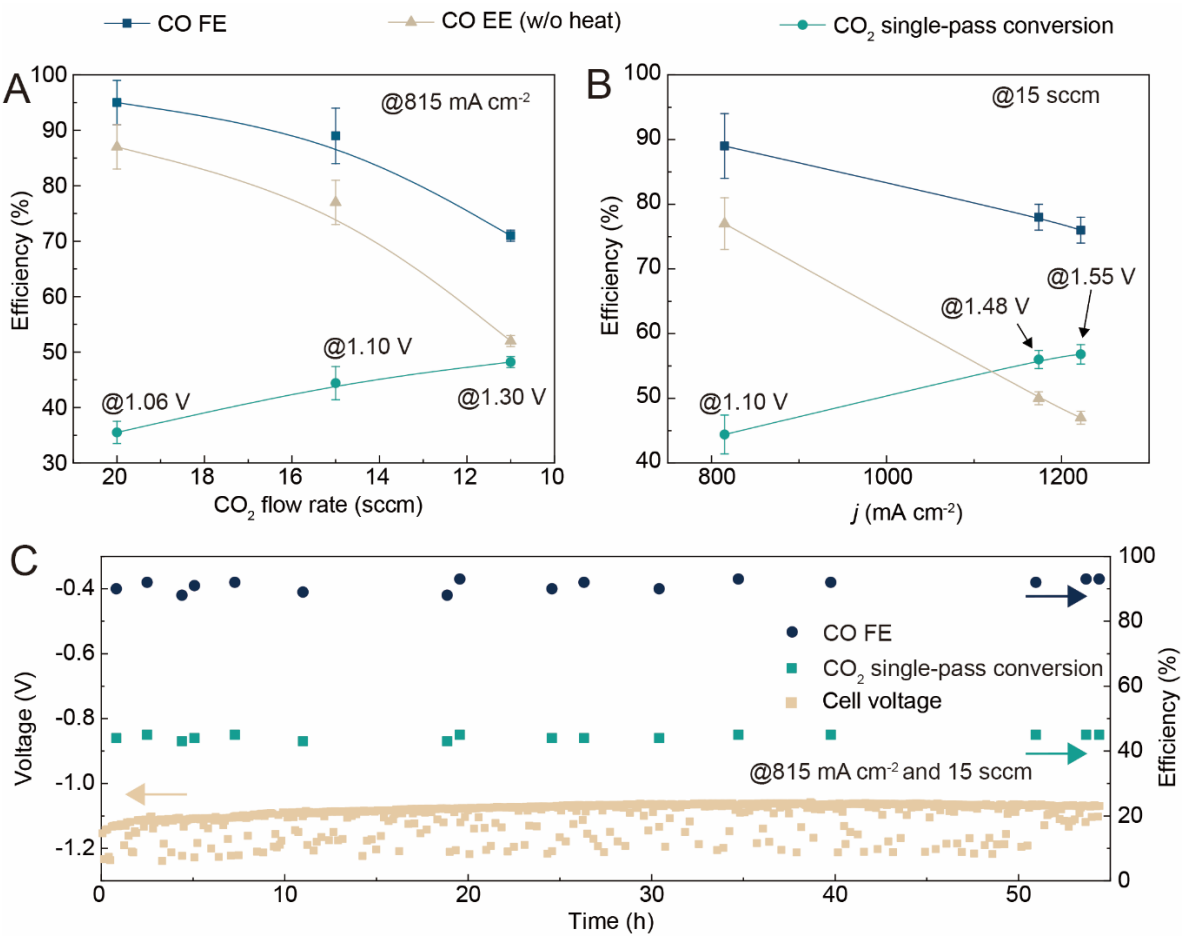

Figure 2. CO_2-to-CO conversion in an SOEC. (A,B) CO_2-to-CO Faradaic efficiency, single-pass conversion, and energy efficiency in a commercial 2.5-cm NiO-YSZ/YSZ/GDC/LSC at various CO_2 flow rates and current densities. The increase in the CO_2 single-pass conversion by lowering CO_2 flow rates or increasing current density was caused by the CO disproportionation reaction, which is also known as the Boudouard reaction. **(C)** The CO_2-to-

CO Faradaic efficiency, single-pass conversion, and cell voltage profiles during 55-hour test at 815 mA cm^{-2} and a CO_2 flow rate of 15 sccm. The operating temperature is 800 °C. The error bars correspond to the standard deviation of three independent measurements.

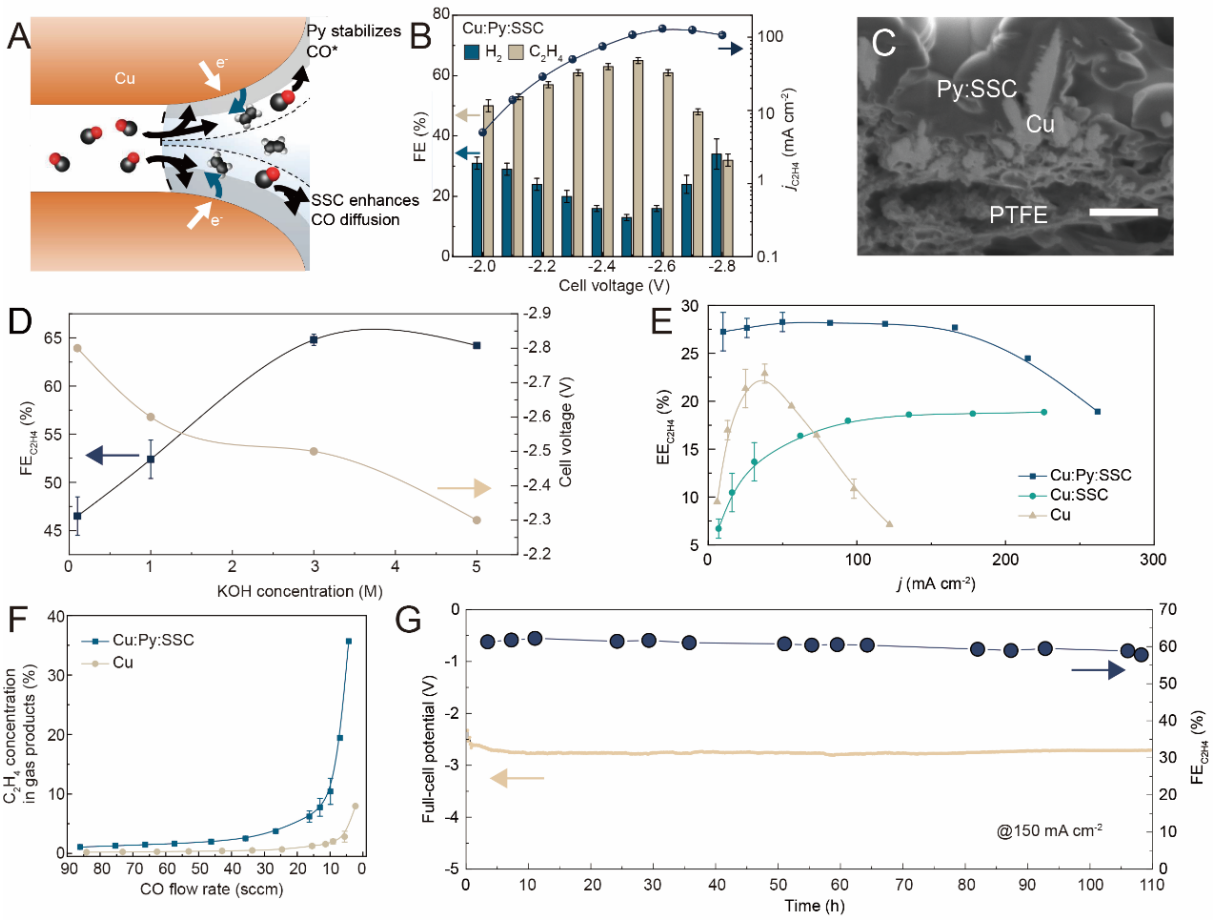

Figure 3. CO-to-C_2H_4 electroreduction in an MEA. (A,B) Introducing additives to improve CO diffusion and stablize CO* intermediates leads to enhanced C_2H_4 selectivity and activity. **(C)** Cross-sectional SEM images of the Cu:Py:SSC catalyst. The scale bar is 1 μm. **(D)** The C_2H_4 FE and full-cell voltages in different anolytes. **(E,F)** Comparisons of the CO-to-C_2H_4 EE and the C_2H_4 concentration obtained using the Cu:Py:SSC catalyst and controls in MEAs with 3 M KOH. **(G)** C_2H_4 FE and full-cell voltage of the MEA equipped with a Cu:Py:SSC cathode for 110 hours at 150 mA cm^{-2}. The error bars correspond to the standard deviation of three independent measurements.

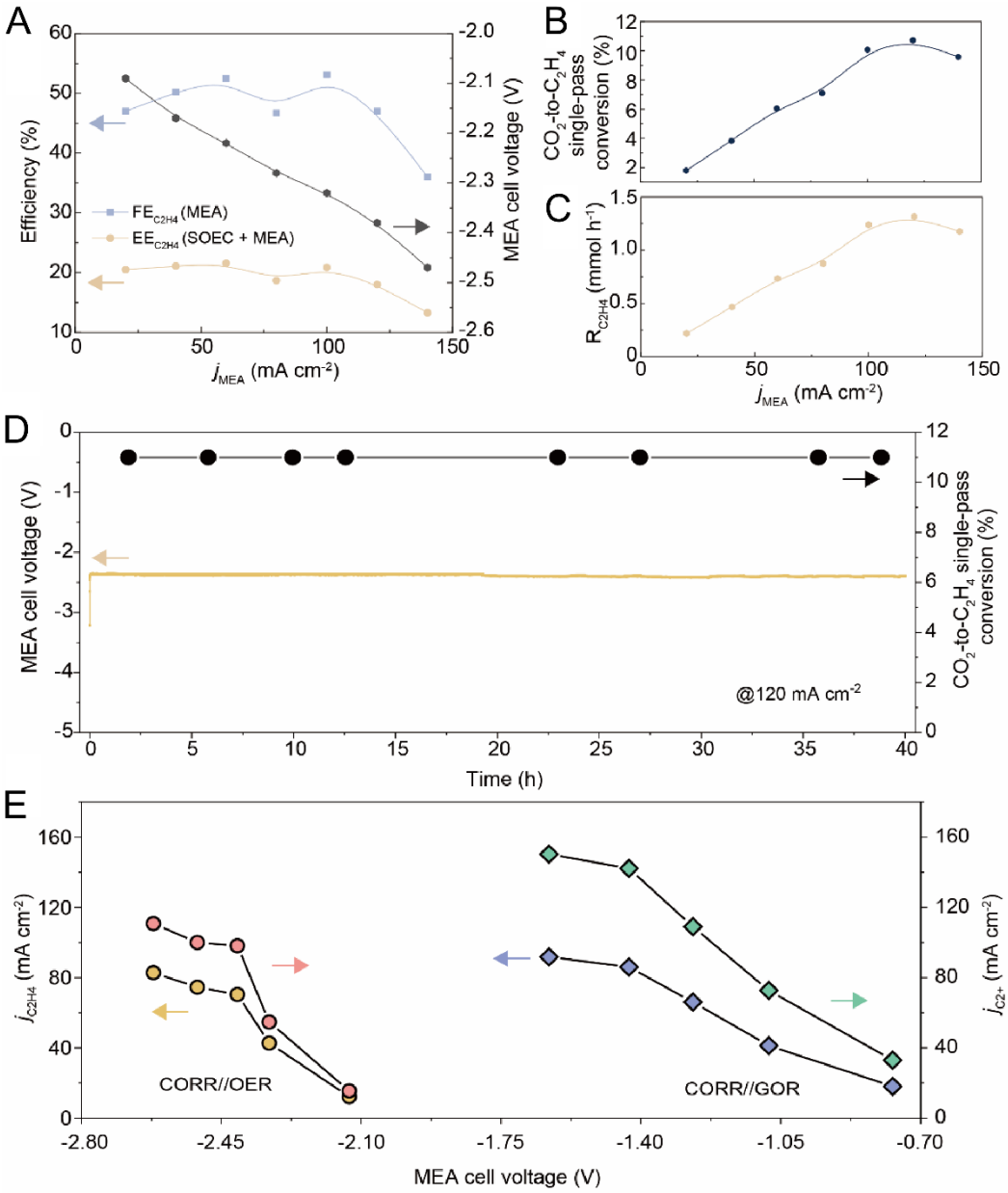

Figure 4. C_2H_4 production performance in the cascade CO_2RR. (A) The C_2H_4 FE and cell voltage of the CO-to-C_2H_4 MEA in the cascade CO_2RR, and the C_2H_4 EE of the cascade CO_2RR. **(B,C)** CO_2-to-C_2H_4 single-pass conversion and C_2H_4 production rates of the cascade CO_2RR at different operating current densities for the CO-to-C_2H_4 MEA. (**D**) Extended CO_2-to-C_2H_4 single-pass conversion performance of the MEA in the cascade CO_2RR. (**E**) Effect of anodic reaction on the CORR performance metrics of the MEA in the cascade CO_2RR.

ACKNOWLEDGMENTS

The authors acknowledge Ontario Centre for the Characterization of Advanced Materials (OCCAM) for sample preparation and characterization facilities. Funding: This work received financial support from the Ontario Research Foundation: Research Excellence Program, the Natural Sciences and Engineering Research Council (NSERC) of Canada, the CIFAR Bio-Inspired Solar Energy program and TOTAL S.E. and the Joint Centre of Artificial Synthesis, a DOE Energy Innovation Hub, supported through the Office of Science of the US Department of Energy under award no. DE-SC0004993. D.S. acknowledges the NSERC E.W.R Steacie Memorial Fellowship. A.T. acknowledges Marie Skłodowska-Curie Fellowship H2020-MSCA-IF-2017 (793471). The authors thank Dr. Y.-F. Liao for the GIWAXS measurements at Spring-8 BL-12B2 beamline of NSRRC. The authors also thank Dr. T. Regier for their assistance at the SGM beamline of CLS.

AUTHOR CONTRIBUTIONS

D.S. and E.H.S. supervised the project. A.O. carried out all the electrochemical experiments with advice from Y.W. and F.L.. A.T., A.R.H., J.C.P., and T.A. designed and synthesized the N-tolylpyridinium molecule and contributed to the manuscript editing. A.O. and F.L. carried out Raman spectroscopies. Y.W. performed the SEM and TEM analysis. A.O. performed the nuclear magnetic resonance spectroscopies. A.O. and Y.W. co-wrote the manuscript. J.S. performed the TEA modelling. T.B. conducted the CO diffusion modelling. M.L., Y.L. and H.Y. contributed to the discussions and manuscript editing. All authors discussed the results and assisted during manuscript preparation.

DECLARATION OF INTERESTS

The authors declare no competing interests.

DATA AVAILABILITY

The data supports the plots within this paper and other findings of this study are available from the corresponding authors upon reasonable request.

REFERENCES

1. Global Data. Global ethylene industry outlook to 2023 – capacity and capital expenditure forecasts with details of all active and planned plants. (2019).
2. Ren, T., Patel, M.K., Blok, Kornelis. Steam cracking and methane to olefins: Energy use, CO2 emissions, and production costs. *Energy* **33,** 817-833 (2008).
3. Hepburn, C. *et al.* The technological and economic prospects for CO_2 utilization and removal. *Nature* **575,** 87-97 (2019).
4. Luna, P.D. *et al.* What would it take for renewably powered electrosynthesis to displace petrochemical process? *Science* **364,** eaav3506 (2019).
5. Dinh C.T. *et al.* CO_2 electroreduction to ethylene via hydroxide-mediated copper catalysis at an abrupt interface. *Science* **360,** 783-787 (2018).
6. Li, F. *et al.* Molecular tuning of CO_2-to-ethylene conversion. *Nature* **577,** 509-513 (2020).
7. Wang, Y. *et al.* Copper nanocubes for CO_2 reduction in gas diffusion electrodes. *Nano Lett.* **19,** 8461-8468 (2019).
8. Ripatti, D.S., Veltman, T.R., Kanan M.W. Carbon monoxide gas diffusion electrolysis that produces concentrated C_2 products with high single-pass conversion. *Joule* **3,** 240-256 (2019).
9. Jouny, M., Hutchings, G.S., Jiao, F. Carbon monoxide electroreduction as an emerging platform for carbon utilization. *Nat. Catal.* **2,** 1062-1070 (2019).
10. Liu, Z., Yang, H., Kutz, R., Masel, R.I. CO2 electrolysis to CO and O_2 at high selectivity, stability and efficiency using sustainion membranes. *Electrochem. Soc.* **165,** J3371-J3377 (2018).
11. Gabardo C.M. *et al.* Continuous carbon dioxide electroreduction to concentrated multi-carbon products using a membrane electrode assembly. *Joule* **3,** 2777-2791 (2019).
12. Wang, L. *et al.* Selective reduction of CO to acetaldehyde with CuAg electrocatalysts. *Chem. Eng. World* **52,** 44-46 (2017).
13. Skafte, T.L., Blennow, P., Hjelm, J., Graves, C. Carbon deposition and sulfur poisoning during CO_2 electrolysis in nickel-based solid oxide cell electrodes. *J. Power. Sources* **373,** 54-60 (2018).
14. Navasa, M., Frandsen, H.L., Skafte, T.L., Sunden, B., Graves, C. Localized carbon deposition in solid oxide electrolysis cells studied by multiphysics modeling. *J. Power. Sources* **394,** 102-113 (2018).
15. Wang, Y. *et al.* Catalyst synthesis under CO_2 electroreduction favours faceting and promotes renewable fuels electrosynthesis. *Nat. Catal.* **3,** 98-106 (2020).
16. Pérez-Gallent, E., Marcandalli, G., Figuiredo, M.C., Calle-Vallejo, F., Koper, M.T.M. *J. Am. Chem. Soc.* **139,** 16412-16419 (2017).

17. Wakerley, D. *et. al.* Bio-inspired hydrophobicity promotes CO2 reduction on a Cu surface. *Nat. Mater.* **18,** 1222-1227 (2019).
18. Schalenbach, M. *et. al.* Gas permeation through Nafion. Part 1: Measurements. *J. Phys. Chem. C* **119,** 25145-25155 (2015).
19. Subbaraman, R., Strmcnik, D., Stamenkovic, V., Markovic, N.M. Three Phase Interfaces at Electrified Metal−Solid Electrolyte Systems 1. Study of the Pt(hkl)−Nafion Interface. *J. Phys. Chem. C* **114,** 8414-8422 (2010).
20. Arquer, F.P.G.d., et. al. CO2 electrolysis to multicarbon products at activities greater than 1 A cm^{-2}. *Science* **367,** 661-666 (2020).
21. Jones, D. Perfluorosulfonic acid membranes for fuel cell and electrolyser applications. Mater. Matters 10, 42 (2015).
22. Han, Z., Kortlever, R., Chen, H-Y., Peters, J.C., Agapie, T. CO2 Reduction Selective for $C_{\geq 2}$ Products on Polycrystalline Copper with N-Substituted Pyridinium Additives. *ACS Cent. Sci.* **3,** 853-859 (2017).
23. Gunathunge, C.M. et. al. Spectroscopic observation of reversible surface reconstruction of copper electrodes under CO_2 reduction. *J. Phys. Chem. C* **121,** 12337-12344 (2017).
24. Heyes, J., Dunwell, M., Xu, B. CO2 reduction on Cu at low overpotentials with surface-enhanced in situ spectroscopy. *J. Phys. Chem. C* **120,** 17334-17341 (2016).
25. Akemann, W., Otto, A. Vibrational modes of CO adsorbed on disordered copper films. *J. Raman Spectrosc*. **22,** 797-803 (1991).
26. Pérez-Gallent, E., Marcandalli, G., Figueiredo, M.C., Calle-Vallejo, F., Koper, M.T.M. *J. Am. Chem. Soc.* **139,** 16412-16419 (2017).
27. Pérez-Gallent, E., Figueiredo, M.C., Calle-Vallejo, F., Koper, M.T.M. Spectoscopic observation of a hydrogenated CO dimer intermediate during CO reduction on Cu(100) electrodes. *Angew. Chem. Int. Ed.* **129,** 3675-3678 (2017).
28. Cheng, T., Xiao, H., Goddard III, W.A. Full atomistic reaction mechanism with kinetics for CO reduction on Cu(100) from ab initio molecular dynamics free-energy calculations at 298 K. *Proc. Natl. Acad. Sci.* **114***,* 1795-1800 (2017).
29. Gunathunge, C.M., Ovalle, V.J., Li, Y., Janik, M.J., Waegele, M.M. Existence of an electrochemically inert CO population on Cu electrodes in alkaline pH. *ACS Catal.* **8,** 7507-7516 (2018).
30. Oda, I., Ogasawara, H., Ito, M. Carbon monoxide adsorption on copper and silver electrodes during carbon dioxide electroreduction studied by infrared reflection absorption spectroscopy and surface-enhanced raman spectroscopy. *Langmuir* **12,** 1094-1097 (1996).
31. Wutting, A. et. al. Tracking a common surface-bound intermediate during CO2-to-fuels catalysis. *ACS Cent. Sci.* **2,** 522-528 (2016).
32. Liu, X. *et. al.* pH effects on the electrochemical reduction of $CO_{(2)}$ towards C_2 products on stepped copper. *Nat. Commun.* **10,** 32 (2019).
33. Jouny, M., Luc, W., Jiao, F. High-rate electroreduction of carbon monoxide to multi-carbon products. *Nat. Catal.* **1,** 748-755 (2018).
34. Aeshala, L.M., Uppaluri, R.G., Verma, A. Effect of cationic and anionic solid polymer electrolyte on direct electrochemical reduction of gaseous CO_2 to fuel. *J. CO_2 Util.* **3,**

49-55 (2013).
35. Merino-Garcia, I., Albo, J., Solla-Gullon, J., Montiel, V., Irabien, A. Cu oxide/ZnO-based surfaces for a selective ethylene production from gas-phase CO_2 electroconversion. *J. CO_2 Utili.* **31,** 135-142 (2019).
36. Merino-Garcia, I., Albo, J. Irabien, A. Productivity and selectivity of gas-phase CO2 electroreduction to methane at copper nanoparticle-based electrodes. *Energy Technol.* **5,** 922-9238 (2017).
37. Verma, S., Lu, S., Kenis, P.J.A. Co-electrolysis of CO2 and glycerol as a pathway to carbon chemicals with improved technoeconomics due to low electricity comsumption. *Nat. Energy* **4,** 466-474 (2019).